Spectral Shape Analysis of the Hippocampal Structure for Alzheimer's Disease Diagnosis

G. Maicas, A.I. Muñoz, G. Galiano, A. Ben Hamza, and E. Schiavi, for the Alzheimer's Disease Neuroimaging Initiative

Abstract We present an automatic pipeline for spectral shape analysis of brain subcortical hippocampal structures with the aim to improve the Alzheimer's Disease (AD) detection rate for early diagnosis. The hippocampus is previously segmented from volumetric T1-weighted Magnetic Resonance Images (MRI) and then it is modelled as a triangle mesh (Fang and Boas, Proceedings of IEEE international symposium on biomedical imaging, pp 1142–1145, 2009) on which the spectrum of the Laplace-Beltrami (LB) operator is computed via a finite element method (Lai, Computational differential geometry and intrinsic surface processing. Doctoral dissertation. University of California, 2010). A fixed number of eigenpairs is used to compute, following (Li and Ben Hamza, Multimed Syst 20(3):253–281, 2014), three different shape descriptors at each vertex of the mesh, which are the heat kernel signature (HKS), the scale-invariant heat kernel signature (SIHKS) and the wave kernel signature (WKS). Each of these descriptors is used separately in a Bag-of-Features (BoF) framework. In this preliminary study we report on the implementation of the proposed descriptors using ADNI (adni.loni.usc.edu), and DEMCAM (T1-weighted MR images acquired on a GE Healthcare Signa HDX 3T scanner) datasets. We show that the best quality of the DEMCAM dataset images

Data used in preparation of this article were obtained from the Alzheimer's Disease Neuroimaging Initiative (ADNI) database (adni.loni.usc.edu). As such, the investigators within the ADNI contributed to the design and implementation of ADNI and/or provided data but did not participate in analysis or writing of this report. A complete listing of ADNI investigators can be found at: http://adni.loni.usc.edu/wp-content/uploads/how_to_apply/ADNI_Acknowledgement_List.pdf

G. Maicas • A.I. Muñoz (✉) • E. Schiavi
Departamento de Matemática Aplicada, Ciencia e Ingeniería de Materiales y Tecnología Electrónica, Universidad Rey Juan Carlos, ESCET, Móstoles, 28933 Madrid, Spain
e-mail: g.maicas@alumnos.urjc.es; anaisabel.munoz@urjc.es; emanuele.schiavi@urjc.es

G. Galiano
Departamento de Matematicas, Universidad de Oviedo, Oviedo 33007, Spain
e-mail: galiano@uniovi.es

A. Ben Hamza
Concordia Institute for Information Systems Engineering, Concordia University, Montreal, Canada, QC
e-mail: hamza@ciise.concordia.ca

have a great impact on the AD rate of detection which can reach up to 95 %. For further development of the modelling approach, local deformation analysis is also considered through a spectral segmentation of the hippocampal structure.

1 Introduction

Alzheimer's disease (AD) is the most common form of cognitive disability in older people, and the number of affected patients is expected to considerably increase in the next future due to the population longer living. Early diagnosis of AD would greatly benefit the public health and society, resulting in patient quality of life and reduced treatment costs.

The development of magnetic resonance images (MRI) has given rise to a deeper study of the architecture of the human body. More precisely, diagnosis of Alzheimer's disease has benefited from this fact due to the possibility of studying the structure of the different components of the brain which show anatomical changes as the disease advances (see for example [18]).

The hippocampus, which is located in the medial temporal lobe of the brain, and is important for memory and spatial navigation, has been shown as one of the main components of the brain that changes in the progression of AD [1]. Its atrophy due to neurodegenerative diseases such as AD can be evaluated in terms of the global change in the volume of the hippocampus as well as through the quantification of the global and local changes in its shape. Hippocampal volumetry on MR images has been shown to be a useful tool in AD diagnosis, providing significant discrimination ability. It is, however, inadequate to fully describe the effect of the disease on the morphology of hippocampus. In addition to volumetry, hippocampal shape analysis is an emerging field enlarging the understanding of the development of the disease. Among the different methods employed to model the hippocampus and to detect the shape changes (deformation) caused by AD, shape surface processing represented by spherical harmonics [8] and statistical shape models (SSMs) have been proved to be efficient in modeling the variability in the hippocampal shapes among the population [16].

In this work, we primarily focus on spectral techniques based on the Laplace-Beltrami operator. Such techniques have been successfully applied to shape recognition of subcortical structures [10]. In [19] a heat kernel based cortical thickness estimation algorithm, which is driven by the graph spectrum and the heat kernel theory, is used to capture grey matter geometry information from in vivo brain MR. These approaches allow to compute some shape spectral descriptors such as the heat kernel signature (HKS), the scale invariant heat kernel signature (SIHKS) and wave kernel signature (WKS), which we apply to the ADNI and DEMCAM datasets. In order to assist the diagnosis of Alzheimer we merge the spectral analysis into a Bag of Features (BoF) (see [13] for details) framework proposed in [11] for shape retrieval. The diagnosis (discrimination) is then effected in the space of descriptors through the comparison of their histograms. Finally we propose a novel method

for anatomical structure segmentation based on the decreasing rearrangement of the second eigenfunction of the Laplace-Beltrami (LB) operator. As an application, we consider a partition of the hippocampus into three regions exploring if just one of them mostly encapsulate the early damages caused by this dementia.

The rest of this paper is organized as follows. In Sect. 2, we consider the heat equation on a closed surface, introducing the LB operator on compact manifolds. In order to expand the solution into eigenfunctions of the LB operator we define its discretization using FEM which leads to solve a generalized eigenvalue problem. In Sect. 3, the BoF approach for shape recognition is presented and the three different shape descriptors are introduced. Local analysis is performed in Sect. 4 through a spectral segmentation algorithm which exploits the properties of the decreasing rearrangement of a function. The experiments and results obtained are described in Sect. 5. Finally we summarize the conclusions of our study which is an ongoing research in the framework of Project TEC2012-39095-C03-02: Mathematical Models based on Biomarkers.

2 Spectral Analysis of the LB Operator

The heat diffusion process has recently been applied successfully to shape recognition [10, 11]. In this section, we present the heat equation and eigenvalue problem on a compact manifold representing the hippocampus surface. We discretize the heat equation in a triangular mesh, which is automatically generated (see [5]) in order to find the LB spectrum using FEM.

Assume $\mathscr{M} \subset \mathscr{R}^3$, where $\mathscr{R}$ denotes the set of real numbers, to be a compact connected Riemannian manifold. Then, the heat diffusion process in the manifold is described by the following equation

$$u_t = \Delta_{\mathscr{M}} u, \qquad \forall\, (\mathbf{x}, t) \in \mathscr{M} \times [0, \infty) \tag{1}$$

$$u(\mathbf{x}, 0) = f(\mathbf{x}), \qquad \forall\, \mathbf{x} \in \mathscr{M} \tag{2}$$

where the scalar field $u : \mathscr{M} \times [0, \infty) \to \mathscr{R}$ is the amount of heat at a point on the surface (hippocampus) at time t, and $\Delta_{\mathscr{M}}$ is the LB operator defined as follows:

$$\Delta_{\mathscr{M}} f = div_{\mathscr{M}}(\nabla_{\mathscr{M}} f) = \frac{1}{\sqrt{G}} \sum_{i=1}^{2} \frac{\partial}{\partial x^i} \left(\sqrt{G} \sum_{j=1}^{2} g^{ij} \frac{\partial f}{\partial x^j} \right),$$

where $G = \det(g_{ij})$ and (g^{ij}) is the inverse of the metric matrix. Considering $u(\mathbf{x}, 0) = \delta(\mathbf{x} - \mathbf{y})$, the solution $k(\mathbf{x}, \mathbf{y}, t)$ of the Eq. (1) is called the heat kernel (HK), which is a measure of the amount of heat that moves from $\mathbf{x}$ to $\mathbf{y}$ after time t.

The HK corresponding to the solution to problem (1)–(2) can be expressed as

$$k(\mathbf{x}, \mathbf{y}, t) = \sum_{i=1}^{\infty} e^{-\lambda_i t} \phi_i(\mathbf{x}) \phi_i(\mathbf{y}). \tag{3}$$

where (λ_i, ϕ_i) are the eigenpairs (spectrum) of the LB operator. Notice that being the manifold closed, we find that $\lambda_1 = 0$ and the first eigenfunction ϕ_1 is constant. The rest of the eigenvalues satisfy $0 < \lambda_2 < \lambda_3 < \ldots$, being this sequence diverging.

In order to expand the solution in terms of the eigenpairs, we need to solve first the following eigenvalue problem:

$$\Delta_{\mathscr{M}} \phi_n = -\lambda_n \phi_n, \qquad n = 1, 2, \cdots. \tag{4}$$

Instead of solving the previous eigenvalue problem, we use a finite element method (FEM) to find numerically an approximate solution in a triangular mesh [10].

Hence, we consider the following weak formulation of the problem: Find $\phi \in H^1(\mathscr{M})$, such that for any test function $u \in H^1(\mathscr{M})$, it is satisfied

$$\int_{\mathscr{M}} (\Delta_{\mathscr{M}} \phi) u \, dV = -\lambda \int_{\mathscr{M}} \phi u \, dV. \tag{5}$$

After the weak formulation for the problem is found, its discretization is the second step according to FEM. Hence, we consider the manifold representing the hippocampus surface as a triangular mesh composed of N vertices and L triangles: $\{V = \{p_i\}_1^N, T^h = \{T_l\}_1^L\}$, where the superindex h refers to the diameter of the triangulation. Let V^h be the space generated by those functions: $V^h = \{u^h \in C(\mathscr{M}) | u_{h|_k} \in \mathscr{P}_1, k \in T^h\}$, where T^h is the set of triangles and $\mathscr{P}_1$ is the set of two-variables linear functions. Each of the elements in V^h is called a linear finite element. Following [10], the discrete version of (5) is: Find $\phi^h \in V^h$ such that

$$\sum_l \int_{T_l} \nabla_{\mathscr{M}} \phi^h \cdot \nabla_{\mathscr{M}} \psi_i^h = \lambda^h \sum_l \int_{T_l} \phi^h \; {}_i^h, \quad \forall \psi_i^h \in S^h,$$

for $i = 1, \ldots, N$, where S^h is a basis of V^h consisting on the element shape functions (Fig. 1).

Considering the following matrices involving every element of the mesh: $\phi^h = \sum_1^N x_i \psi_i^h$, $\mathbf{A}^h = (a_{ij})_{N \times N}$, where $a_{ij} = \sum_l \int_{T_l} \nabla_{\mathscr{M}} \psi_i^h \nabla_{\mathscr{M}} \psi_j^h$, and $\mathbf{B}^h = (b_{ij})_{N \times N}$, with $b_{ij} = \sum_l \int_{T_l} \psi_i^h \psi_j^h$, the variational problem (5) is then equivalent to the following eigenvalue problem:

$$\mathbf{A}^h \mathbf{x} = \lambda^h \mathbf{B}^h \mathbf{x},$$

where $\mathbf{x} = (x_1, \cdots, x_N)^t$ are the unknown associated eigenfunctions (i.e. eigenvectors which can be thought of as functions on the mesh vertices). This gener-

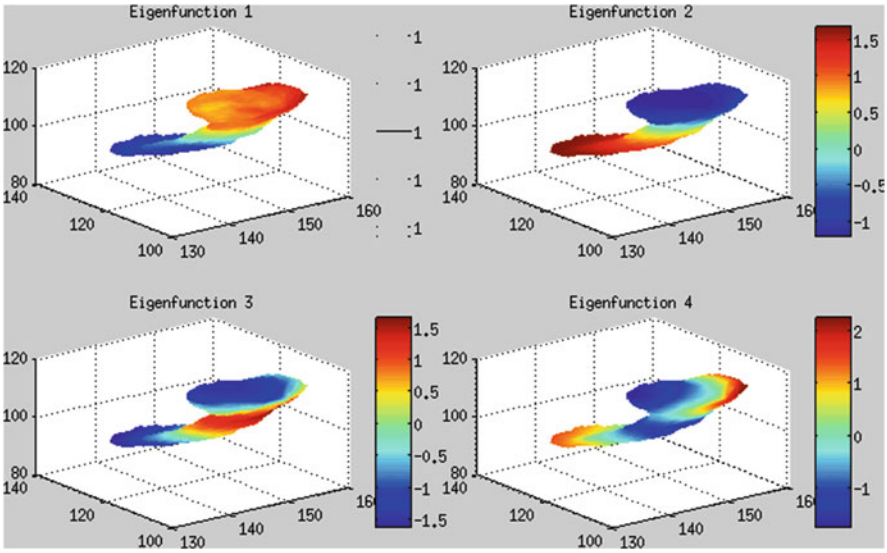

Fig. 1 Representation of the first four eigenfunctions of the LB operator. Notice that the first eigenfunction takes approximately a constant value, as expected. The second eigenfunction is known by capturing well topological features and the geometry of the shape (it corresponds to the sound we hear the best [7])

alized eigenvalue problem may be efficiently solved using the Arnoldi method of ARPACK. The computation of the local integrals $\int_{T_l} \psi_i^h \psi_j^h$ and $\int_{T_l} \nabla_{\mathscr{M}} \psi_i^h \nabla_{\mathscr{M}} \psi_j^h$, is carried out following the ideas presented in [10] based in the use of barycenter coordinates, and which we will briefly describe here. Let T_l be a triangle defined by the vertices $T_l = \{p_0, p_1, p_2\}$, $\psi_i^h \in S^h$ and $\psi_i^h = \{\psi_{i,0}, \psi_{i,1}, \psi_{i,2}\}$ the corresponding values at the vertices of the considered triangle. A point $p \in T_l$ may be expressed in barycenter coordinates as

$$p = x^1(p_1 - p_0) + x^2(p_2 - p_0) + p_0$$

such that $0 \leq x^1, x^2, x^1 + x^2 \leq 1$. For $p \in T_l$, the values of the functions ψ_i and ψ_j might be estimated by using linear interpolation as follows:

$$\overset{h}{i}(p) = x^1(\psi_{i,1} - \psi_{i,0}) + x^2(\psi_{i,2} - \psi_{i,0}) + \psi_{i,0},$$

$$\overset{h}{j}(p) = x^1(\psi_{j,1} - \psi_{j,0}) + x^2(\psi_{j,2} - \psi_{j,0}) + \psi_{j,0}.$$

Therefore, any of the integrals needed to find matrix **B** may be approximated as

$$\int_{T_l} \psi_i^h \ \overset{h}{j} dv = \int_0^1 \int_0^{1-x^1} \overset{h}{i}(p)\psi_j^h(p) dx^2 dx^1.$$

Finally, we need to find an estimation of integrals taking part in the matrix **A** entries. Note that in a linear finite element method, the gradient in each element will be constant vectors. Thus, we may write

$$\int_{T_l} \nabla\psi_j^h \cdot \nabla\psi_i^h dv = area(T_l)(\nabla\psi_i^h|_{T_l} \cdot \nabla\psi_j^h|_{T_l}),$$

where $area(T_l)$ is the area of the element considered. The computation of the gradients $\nabla\psi_i^h|_{T_l}$ and $\nabla\psi_j^h|_{T_l}$, is carried out through the following expression for $\nabla\psi_i^h|_{T_l}$ and analogously for $\nabla\psi_j^h|_{T_l}$ (see [10] for details):

$$\nabla\psi_i^h|_{T_l} = (\psi_{i,1} - \psi_{i,0}, \psi_{i,2} - \psi_{i,0}) \begin{pmatrix} \partial_{x^1} \cdot \partial_{x^1} & \partial_{x^1} \cdot \partial_{x^2} \\ \partial_{x^2} \cdot \partial_{x^1} & \partial_{x^2} \cdot \partial_{x^2} \end{pmatrix}^{-1} \begin{pmatrix} p_1 - p_0 \\ p_2 - p_0 \end{pmatrix}$$

where $\partial_{x^1} = p_1 - p_0$ and $\partial_{x^2} = p_2 - p_0$.

3 Modeling Shapes

Methods for recognizing 3D shapes by their meaningful parts may be broadly divided into two categories. The first, following [11], is the *skeleton based* method (see [9]). The second one, which is the one considered in our study, is the *surface based* method. In the latter case, a shape is modelled as a frequency histogram, which is later used to compare it. The bag of features, the chosen methodology in this work, is an example of methodology that belongs to this group.

3.1 Bag of Features

The bag of features (BoF) paradigm (see [13] for details) is one of the most popular feature-based methods for shape recognition, retrieval and detection. The steps for the BoF methodology are the following: First, we detect and extract features from every shape in the training database. Second, we compute a dictionary of visual words using the training data, and allocate each feature to the closest vocabulary word. Next, we obtain the histogram of frequency for every shape. And finally, given a test shape, we model it as its histogram of frequency using the same signature, and we determine its class by majority voting of the closest training neighbors.

Local descriptors have been proven to perform well on shape recognition tasks. For every training sample, at each point of the mesh, a feature vector is computed. We build different bag of features using each of the following descriptors: the heat kernel signature (HKS), the scale-invariant heat kernel signature (SIHKS) and the wave kernel signature (WKS).

In order to quantize the feature space, the data are clustered using training samples. These data representatives are called vocabulary features. In our study, we use the k-means algorithm (see [12] for details). As each shape is modelled by a histogram, comparing shapes is tantamount to measuring histogram similarity. Two different histograms comparison metrics are used: chi-squared and Spearman distances.

3.2 Shape Descriptors

As introduced before, two different kinds of descriptors will be used: heat-diffusion and wave based descriptors. The former measures the amount of heat that remains in a point of the shape after some time t. Therefore, it is possible to capture shape information using small diffusion times and global characteristics when heat diffuses for a longer time. In addition, several times t or scales will be considered to build a feature vector for each point in the shape. The latter descriptor, which is based on the resolution of the Schrödinger equation, describes a shape by means of the probability of finding a quantum particle at a particular point of the shape.

3.2.1 HKS

At a given point of the mesh $\mathbf{p} \in \mathscr{M}$, the heat left after a time t if initially all of it was concentrated at one point, that is $u(\mathbf{p}, 0) = \delta(\mathbf{p})$, is described by $k(\mathbf{p}, \mathbf{p}, t) = K_t(\mathbf{p}, \mathbf{p})$ (see (3)), where t is the diffusion time or time scale. The heat kernel signature at each $\mathbf{p} \in \mathscr{M}$ is defined as a n-dimensional vector

$$HKS(\mathbf{p}) = (K_{t_1}(\mathbf{p}, \mathbf{p}), \cdots, K_{t_n}(\mathbf{p}, \mathbf{p})), \tag{6}$$

where $t_1, \cdots, t_n$ are different time scales.

The main advantages of the HSK are [4, 14]: it is robust to noise, it is easy to compute as it is based on the first eigenvalues and eigenfunctions, and the HKS of a shape is unique except under isometries. A major drawback of HKS is that it depends on the pixels' volume of the shape, therefore, the same hippocampus in two different scales differs on this descriptor.

3.2.2 SIHKS

In order to overcome the just mentioned dependence of HKS on the scale of the shape, Bronstein and Kokkinos [3] proposed an updated heat kernel signature which is independent on the scale-space. The scale invariant heat kernel signature, SIHKS (see [11]), which we consider in our study has been proven to improve results related to the HKS or the WKS [3, 11]. Next, we shall briefly describe the

derivation of the SIHKS for reader's convenience. Given a shape $\mathscr{M}$, the heat kernel signature at a point $\mathbf{p} \in \mathscr{M}$ at time t is given by (6). Considering the same shape scaled, $\mathscr{M}' = \beta\mathscr{M}$, the relation between the eigenvalues and eigenfunctions of the Laplace-Beltrami operator of the two shapes satisfy $\lambda_i^{'} = \beta^2\lambda_i$ and $\phi_i^{'} = \beta\phi_i$, and the heat kernel signature for each point $\mathbf{p} \in \mathscr{M}'$ at a time t can be written as

$$K_t^{'}(\mathbf{p},\mathbf{p}) = \sum_{i=1}^{\infty} e^{(-\lambda_i\beta^2 t)}\phi_i\phi_i\beta^2 = \beta^2 K_{\beta^2 t}(\mathbf{p},\mathbf{p}). \tag{7}$$

The expression (7) relates the heat kernel signature of a point in the β-scaled version $\mathscr{M}'$ at time t with the descriptor of the non-scaled version of the shape at time $\beta^2 t$. In order to accomplish the scale invariance for the HKS, we need to remove β from (7). For this purpose, we shall first write the HKS in a logarithmic time $t = \alpha^\tau$ for each point $\mathbf{p} \in \mathscr{M}$, $K_\tau = K_{\alpha^\tau}(\mathbf{p},\mathbf{p})$. Hence, in the scaled version of the surface, $\mathscr{M}' = \beta\mathscr{M}$, the heat kernel signature can be written as follows $K_\tau^{'} = \beta^2 K_{2log_\alpha\beta+\tau}$, and (7) is translated into

$$K_\tau^{'} = \beta^2 K_{\tau+s} \tag{8}$$

where $s = 2log_\alpha\beta$. Now, taking logarithms in (8) and derivating with respect to τ, we obtain that

$$\frac{d}{d\tau}\log K_\tau^{'} = \frac{d}{d\tau}\log\beta^2 + \frac{d}{d\tau}\log K_{\tau+s} = 0 + \frac{d}{d\tau}\log K_{\tau+s}, \tag{9}$$

where $\frac{d}{d\tau}\log K_\tau^{'}$ will be computed in terms of the eigenpairs of the LB operator, through the following identity:

$$\frac{d}{d\tau}\log K_\tau^{'} = \frac{-\sum_{i\geq 0}\lambda_i\alpha^\tau\log\alpha e^{-\lambda_i\alpha^\tau}\phi_i^2}{-\sum_{i\geq 0}e^{-\lambda_i\alpha^\tau}\phi_i^2}. \tag{10}$$

Taking the discrete Fourier transform in (9) to obtain $FK^{'}(\omega) = FK(\omega)e^{2\pi\omega s}$, and computing the modulus of the Fourier transform, we find $|FK^{'}(\omega)| = |FK(\omega)|$. Therefore, $|FK(\omega)|$ is scale-invariant, and we can consider the scale-invariant heat kernel signature at each $\mathbf{p} \in \mathscr{M}$ defined as a n-dimensional vector

$$SIHKS(\mathbf{p}) = (|FK(\omega_1)|,\cdots,|FK(\omega_n)|),$$

for different frequencies $\omega_1,\ldots,\omega_n$.

3.2.3 WKS

Instead of building a descriptor based on the heat diffusion on the manifold, Aubry et al. [2] proposed a signature, the wave kernel signature (WKS), based on the

consideration of the Schrödinger equation

$$\frac{\partial \psi}{\partial t}(\mathbf{x}, t) = i\Delta_{\mathscr{M}}\psi(\mathbf{x}, t),$$

whose solution is a wave function which describes quantum aspects of a system. Hence, the use of WKS is in fact a quantum approach to shape analysis.

Next, we shall present a basic description of the WKS (see [2, 11] for more details). The basic idea is to characterize a point $\mathbf{p} \in \mathscr{M}$ by the average probabilities over time of quantum particles of different energy levels to be measured in $\mathbf{p}$. So, let f_E^2 be an energy probability distribution of the estimated energy E at time $t = 0$ of a quantum particle which position on the manifold is not known. Then, the wave function of the particle $\psi_E(x, t)$, if there are no repeated eigenvalues of the Laplace-Beltrami operator, can be written as

$$_E(\mathbf{x}, t) = \sum_{k=0}^{\infty} e^{iE_k t}\phi_k(\mathbf{x})f_E(E_k), \tag{11}$$

where $\{(E_k, \phi_k(\mathbf{x}))\}$ are the eigenpairs of the Laplace-Beltrami operator, which represent the energy levels of the quantum system (eigenvalues) and the corresponding wave functions (eigenfunctions) which describe the associated energy state. In fact, the probability to measure a particle at the point of the manifold $\mathbf{p} \in \mathscr{M}$, is $|\psi_E(\mathbf{p}, t)|^2$. Due to the fact that the time parameter has not clear interpretation in our analysis, it will be not taken into consideration when defining the WKS. Then, the wave kernel signature at a point $\mathbf{p}$ of the manifold $\mathscr{M}$, is the probability to measure a quantum particle overtime in an energy level

$$WKS(E, \mathbf{p}) = \lim_{T\to\infty} \frac{1}{T}\int_0^T |\psi_E(\mathbf{p}, t)|^2 dt, \tag{12}$$

which can be written as

$$WKS(E, \mathbf{p}) = \sum_{k=0}^{\infty} \phi_k^2(\mathbf{p})f_E^2(E_k). \tag{13}$$

Regarding the energy distributions f_E^2, in [2] it is discussed that the log-normal probability distribution for f_E^2 models well the energies for our purpose. Therefore, we choose f_E^2 to be a Gaussian distribution in the logarithmic scale. Considering a logarithmic energy scale $sc = log(E)$, the wave kernel signature at $\mathbf{p} \in \mathscr{M}$ is defined as follows:

$$WKS(sc, \mathbf{p}) = C_{sc}\sum_k \phi_k^2(\mathbf{p})e^{\frac{-(sc-\log E_k)^2}{2\sigma^2}}, \tag{14}$$

where C_{sc} is the normalizing constant $C_{sc} = \left(\sum_k e^{\frac{-(sc - \log E_k)^2}{2\sigma^2}} \right)^{-1}$. We obtain an n-dimensional vector by considering different values for *sc* (different energy levels) as well as σ.

Two important properties led us to include this descriptor in out study. First, it is invariant under isometries. In addition, if two shapes have the same WKS for every point of it, then both shapes are the same except for an isometry. Secondly, it is robust to noise, scale or holes in the shape.

4 Local Deformation

Recent findings suggest that the deformations on the hippocampus due to AD do not occur uniformly [19]. This leads to the necessity to develop local deformation analysis and an attempt is done here where we spectrally segment the hippocampus into different regions (classes).

We propose to apply the Neighborhood filter (NF) in terms of the decreasing rearrangement, which has recently been applied to image segmentation in [6]. In order to find a spectral segmentation of the hippocampus, we apply this technique to the quantized values of the second eigenfunction, since it is the first eigenfunction which does not take a constant value and it captures well topological features and the geometry of the shape (see [11]). In fact, the second eigenfunction of the LB operator follows the pattern of the overall shape of an object, and this geometric property is well known and used for various applications including mesh processing, feature extraction, manifold learning, data embedding, etc. (see [17]).

It is important to remark that this technique is computationally extremely efficient because the integrals involved are 1-dimensional. After applying the NF, the fixed point solution is a staircasing piecewise constant function which defines, through thresholding, a partition of the hippocampus into regions (classes) where each one of them can be understood as a segmentation of the initial shape [6].

5 Experimental Results

In our experiments we compare hippocampi using the BoF built with the three different spectral shape descriptors that we described in Sect. 3. Our aim is to achieve an acceptation rate around 80 % or above, as volume or surface area discriminate up to 80 %.

We classify hippocampi according to two disjoint classes: AD and control. To evaluate similarity between shapes, we consider two different histogram metrics, which are the chi-squared and Spearman distances. We use a total of seven

eigenpairs of the LB operator to construct the descriptors. Experimentally we found that no clear improvement is achieved when using a larger number.

5.1 Database

In order to carry out our analysis, we used two datasets.

DEMCAM The DEMCAM project was a research initiative developed in Madrid for Alzheimer's dementia early detection. This dataset was collected from several hospitals of Madrid. It consists of 38 subjects, 19 control patients and 19 patients suffering from Alzheimer's disease. A total of nine subjects from each class are used as training data and the rest is test data. For each subject, a 3D high-resolution T1-weighted MR image was acquired on a GE Healthcare Signa HDX 3T scanner. All original MRIs were automatically segmented using FreeSurfer, which process included a bias field correction (N3 algorithm). Using the open source software *iso2mesh*, we obtained the left and right hippocampus represented as a triangular mesh. This mesh is described by its faces (triangles) and their vertices (Fig. 2).

ADNI The ongoing Alzheimer's disease Neuroimaging Initiative (ADNI) has been designed to provide researchers a common data framework to help in the evaluation of new methods in Alzheimer's disease detection. We considered a total of 180

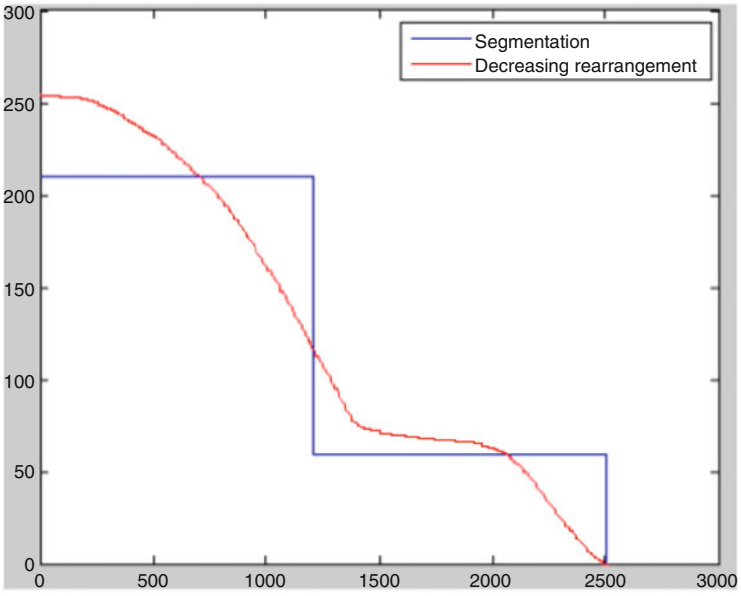

Fig. 2 NF-Decreasing rearrangement of the second eigenfunction of the Laplace-Beltrami operator quantized in 256 levels for a control hippocampus

subjects, 90 healthy patients and 90 ill subjects. We built a test data of 100 samples, including 50 of each category. Forty of the remaining patients were used as training data. Notice that the field strength (1.5T) is lower in ADNI than in DEMCAM (3T). This fact will affect the rates of AD detection.

ADNI data used in the preparation of this article were obtained from the Alzheimer's Disease Neuroimaging Initiative (ADNI) database (adni.loni.usc.edu). The ADNI (Principal Investigator Michael W. Weiner, MD) began in 2003 as a public-private partnership. The aim of ADNI has been to test whether serial magnetic resonance imaging (MRI), positron emission tomography (PET), other biological markers, and clinical and neuropsychological assessment can be combined to describe the development of mild cognitive impairment (MCI) and early Alzheimer's disease (AD).

Next, we present the experimental results obtained with the two datasets considering for classification just the left hippocampus, just the right hippocampus or the whole hippocampal structure.

5.2 DEMCAM Database

It is remarkable that SIHKS achieves the best performance with an acceptance rate of 95 % when considering both hippocampi. It outperforms WKS (90 % when considering information only of right hippocampi) and HKS (85 % when taking into account information from both hippocampi). In addition, as we expected, more information is captured by combining descriptors from both left and right hippocampi in the case of SIHKS and HKS. However, WKS uses right hippocampi to distinguish better healthier from dementia patients. This suggests that combining information leads to a better detection and also that the right hippocampus is more damaged by this disease. In fact, right hippocampus detection outperforms left hippocampus diagnosis in the maximum acceptance rates we obtained for SIHKS, WKS and HKS (see Table 1).

Table 1 Acceptance rates (%) with the standard BoF using HKS, SIHKS and WKS for DEMCAM data

DEMCAM	HKS	SIHKS	WKS
Left hippocampus	65	80	70
Right hippocampus	80	90	90
Joined	85	**95**	85

5.3 ADNI Database

Once again, SIHKS yields the best performance by correctly identifying 80 % of cases. As it was expected, information from both hippocampi (left and right) is taken into account in this outcome. HKS correctly classified 78 % of cases while WKS obtained 74 %. Also, these maxima are achieved when combining information from both left and right hippocampi (see Table 2). Regarding histogram similarity, the results show that Spearman distance leads to obtain the maximum performance for all signatures, as it occurs when considering the DEMCAM dataset.

Therefore, from this study we can argue that the scale-invariant heat kernel signature is the most suitable descriptor for detecting Alzheimer's disease. This conclusion is in agreement with [11] where it is stated that SIHKS outperformed the HKS and the WKS in most cases for shape retrieval.

5.4 Local Deformation Analysis

In order to find which zone of the hippocampus encodes more information for identifying Alzheimer's disease, we spectrally divide hippocampi into three regions, applying the Neighborhood filter (NF) in terms of the decreasing rearrangement.

We consider the zones detailed in Fig. 3 to build a BoF for each of the descriptors. In Table 3 we present the acceptance rates obtained for ADNI data for each of the just mentioned zones. The results show that SIHKS encodes most of the information for detecting Alzheimer's disease from zone 3. Region analysis using WKS as signature describes a similar behavior because encoding information from just region 2 outperforms the general WKS approach by 1 %. On the other hand, no clear information is obtained by using the HKS for local analysis. Nevertheless, 71 % of hippocampi were assigned correctly its class just by considering region 2. This descriptor needs a more global information of the shape for an accurate diagnosis. Following [11] we also model each shape by concatenating histograms corresponding to zones one, two and three, but this does not improve the descriptor performances.

Table 2 Acceptance rates (%) with the standard BoF using HKS, SIHKS and WKS for ADNI data

ADNI	HKS	SIHKS	WKS
Left hippocampus	76	71	67
Right hippocampus	68	78	73
Joined	78	**80**	74

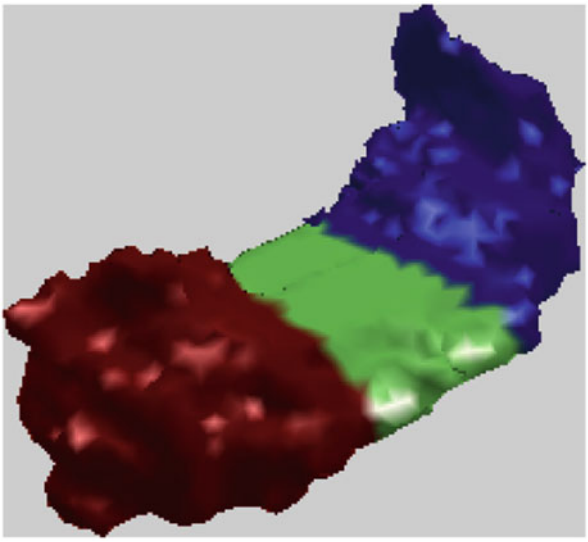

Fig. 3 Segmentation (partition) of a hippocampus into three classes using the NF in terms of the decreasing rearrangement. Zone 1: *blue-colored region*. Zone 2: *green-colored region*. Zone 3: *red-colored region*

Table 3 Acceptance rates (%) for each region of the hippocampus detailed in Fig. 3, with the standard BoF using HKS, SIHKS and WKS for ADNI data

ZONE	HKS	SIHKS	WKS
1	67	69	65
2	**71**	72	**75**
3	70	**78**	59
Concatenating	**72**	**78**	73

5.5 Preprocessing

In order to evaluate the effect of a preprocessing step in the hippocampus and to analyze if the noise removal involves an improvement in the detection rates of AD, we use the smoothing approach technique described in [15]. To be precise, we solve numerically the diffusion equation on the hippocampus by means of the convolution of the heat kernel, expressed as a series expansion of the eigenpairs of the LB operator, with the signal consisting of the coordinates of each of the vertices of the manifold.

According to our observations, no increase of performance is achieved by smoothing hippocampi. In fact, SIHKS and WKS best performances decreased, while HKS best acceptation rates remain constant [2]. This results suggests that the three signatures are robust to small rates of topological noise. This property is very important due to the fact that segmentation of the hippocampi from MRI may include noise. Therefore, it seems not to be necessary to apply a preprocessing step before building the BoF, which prevents from losing small details and saves computation time. In addition, the lack of precise hippocampi extraction from MRI may influence the performance of the techniques used here, as automatic segmentation of the hippocampus might not include important details to detect AD.

6 Conclusions

In this paper, we presented the use of three descriptors, namely HKS, SIHKS and WKS, in the bag-of-features framework for automatic detection of Alzheimer's disease. Our results showed that SIHKS is the best signature in detecting Alzheimer's disease in the proposed framework for both datasets. When the whole hippocampi structure is considered, the performance of our method further increases.

In an effort to study if the hippocampal structure is deformed uniformly or any of the regions is most damaged by this dementia, we proposed a spectral segmentation method of the hippocampus based on the reformulation of a NF using the decreasing rearrangement. Our preliminary results suggest that local analysis deformation usually detects a region with a greater discriminative power, but it can be different for various descriptors which makes premature any conclusion. Finally, the detection rates for 3T (DEMCAM) images are relatively greater than for 1.5T images (ADNI), which is a clear evidence that the proposed technique benefits from image quality.

Acknowledgements The second and last two authors would like to thank Ministerio de Economía y Competitividad de España for supporting Project TEC2012-39095-C03-02. Data used in preparation of this article were obtained from the Alzheimer's Disease Neuroimaging Initiative (ADNI) database and from the Hospital Fundación Reina Sofía, Madrid, Spain (DEMCAM dataset).

ADNI data: This project was funded by the Alzheimer's Disease Neuroimaging Initiative (ADNI; NIH Grant U01 AG024904; Principal Investigator: Michael Weiner). ADNI is funded by the National Institute on Aging, the National Institute of Biomedical Imaging and Bioengineering, and through generous contributions from the following: AbbVie, Alzheimer's Association; Alzheimer's Drug Discovery Foundation; Araclon Biotech; BioClinica, Inc.; Biogen; Bristol-Myers Squibb Company; CereSpir, Inc.; Eisai Inc.; Elan Pharmaceuticals, Inc.; Eli Lilly and Company; EuroImmun; F. Hoffmann-La Roche Ltd and its affiliated company Genentech, Inc.; Fujirebio; GE Healthcare; IXICO Ltd.; Janssen Alzheimer Immunotherapy Research & Development, LLC.; Johnson & Johnson Pharmaceutical Research & Development LLC.; Lumosity; Lundbeck; Merck & Co., Inc.; Meso Scale Diagnostics, LLC.; NeuroRx Research; Neurotrack Technologies; Novartis Pharmaceuticals Corporation; Pfizer Inc.; Piramal Imaging; Servier; Takeda Pharmaceutical Company; and Transition Therapeutics. The Canadian Institutes of Health Research is providing funds to support ADNI clinical sites in Canada. Industry contributions are facilitated by the Foundation for the National Institutes of Health (www.fnih.org). The grantee organization is the Northern California Institute for Research and Education, and the study is coordinated by the Alzheimer's Disease Cooperative Study at the University of California, San Diego. ADNI data are disseminated by the Laboratory for Neuro Imaging at the University of Southern California.

References

1. Aguilar, C., Muehlboeck, J.S., Mecocci, P., Velles, B., Tsolaki, M., Kloszewka, I., et al.: Application of a MRI based severity index of longitudinal atrophy change in Alzheimer's disease mild cognitive impairment and healthy older individuals in the AddNeuroMed cohort. Front. Aging Neorosci. **6**(145) (2014)

2. Aubry, M., Schlickewei, U., Cremers, D.: Pose-consistent 3D shape segmentation based on a quantum mechanical feature descriptor. Pattern Recognition, pp. 122–131. Springer, Heidelberg (2011)
3. Bronstein, M.M., Kokkinos, I.: Scale-invariant heat kernel signatures for non-rigid shape recognition. In: Proceedings of the CVPR (2010)
4. Castellani, U., Mirtuono, P., Murino, V., Bellani, M., Rambaldelli, G., Tansella, M., Brambilla, P.: A new shape diffusion descriptor for brain classification. In: Medical Image Computing and Computer-Assisted Interventional MICCAI, pp. 426–433. Springer, Heidelberg (2011)
5. Fang, Q., Boas, D.: Tetrahedral mesh generation from volumetric binary and gray-scale images. In: Proceedings of IEEE International Symposium on Biomedical Imaging, pp. 1142–1145 (2009)
6. Galiano, G., Velasco, J.: Neighborhood filters and the decreasing rearrangement. J. Math. Imaging Vis. 51(2), 279–295 (2015)
7. Gallot, S., Hulin, D., Lafontaine, J.: Riemannian Geometry. Springer, Berlin/Heidelberg (2004)
8. Gerig, G., Styner, M., Jones, D., Weinberger, D., Lieberman, J.: Shape analysis of brain ventricles using SPHARM. In: Proceedings of the IEEE Workshop on Mathematical Methods in Biomedical Image Analysis (MMBIA'01), p. 171. IEEE Computer Society (2001)
9. Kacem, A., Mohamed, W., Ben Hamza, A.: Spectral Geometric Descriptor for Deformable 3D Shape Matching and Retrieval, Image Analysis and Recognition. Lecture Notes in Computer Science, vol. 7950, pp. 181–188. Springer, Berlin (2013). http://dx.doi.org/10.1007/978-3-642-39094-4-21
10. Lai, R.: Computational differential geometry and intrinsic surface processing. Doctoral dissertation. University of California (2010)
11. Li, C., Ben Hamza, A.: Spatially aggregating spectral descriptors for nonrigid 3d shape retrieval: a comparative survey. Multimedia Syst. **20**(3), 253–281 (2014)
12. MacQueen, J.: Some methods for classification and analysis of multivariate observations. In: Proceedings of the Fifth Berkeley Symposium on Mathematical Statistics and Probability, pp. 281–297 (1967)
13. Nowak, E., Jurie, F., Triggs, B.: Sampling strategies for bag-of-features image classification. In: Computer Vision ECCV, pp. 490–503. Springer, Heidelberg (2006)
14. Raviv, D., Bronstein, M.M., Bronstein, A.M., Kimmel, R.: Volumetric heat kernel signatures. In: Proceedings of the ACM Workshop on 3D Object Retrieval, pp. 39–44. ACM, New York (2010)
15. Seo, S., Chung, M.K., Vorperian, H.K.: Heat kernel smoothing using Laplace-Beltrami eigenfunctions. In: Medical Image Computing and Computer-Assisted Intervention-MICCAI, pp. 505–512. Springer, Heidelberg (2010)
16. Shen, K., Fripp, J., Mériandeau, F., Chételat, G., Salvado, O., Bourgeaut, P., Alzheimer's Disease NeuroImaging Initiative: Detecting global and local hippocampal shape changes in Alzheimer's disease using statistical shape models. NeuroImage **59**, 2155–2166 (2012). http://dx.doi.org/10.1016/j.media.2011.10.014
17. Suzuki, K., Wang, F., Shen, D., Yan, P. (eds.): Machine learning in medical imaging. In: Second International Workshop MLMI 2011, Held in Conjunction with MICCAI, Toronto, Canada, Sep 2011 Proceedings. Lecture Notes in Computer Science, vol. 7009 (2011)
18. Teipei, S.J., Born, C., Ewers, M., Bokde, A.L., Reise, M.F., et al.: Multivariate deformation-based analysis of the brain atrophy to predict Alzheimer's disease in mild cognitive impairment. NeuroImage **38**(1), 13–24 (2007)
19. Wang, G., Zhang, X., Su, Q., Shi, J., Caselli, R.J., Wang, Y., for the Alzheimer's Disease NeuroImaging Initiative: A novel cortical thickness estimation method based on volumetric Laplace-Beltrami operator and heat kernel. Med. Image Anal. **22**, 1–20 (2015). http://dx.doi.org/10.1016/j.media.2015.01.005